CBPF-NF-027/98

Investigation of magnetic structure in steels of a system $Fe - Mn - Al - C$ by atomic force microscopy

G.L. Klimchitskaya [*] [**], R. Prioli, S.I. Zanette, and A.O. Caride

Centro Brasileiro de Pesquisas Físicas, Rua Xavier Sigaud, 150, CEP 22290–900, RJ,Brazil

O. Acselrad, I.S. Kalashnikov [***], E.M. Silva, and R.A. Simão

Departamento de Programa de Engenharia Metalurgica e de Materialas, Universidade Federal de Rio de Janeiro, Ilha do Fundão, RJ, Brazil

Abstract

Magnetic force microscopy is used to investigate the magnetic structure of steels $Fe - 28Mn - 8.5Al - 1C - 1.4Si$ under different regimes of isothermal aging. A theoretical model for the magnetic force microscopy imaging of such structures is developed. Calculations of van der Waals forces were performed in order to interpret the topography images. The lateral resolution in terms of the magnetic field dependence on the surface coordinates is also investigated. Conditions that should be fulfilled for a good imaging of the samples are also formulated.

Key-words: AFM; MFM; Magnetic steels.

I. INTRODUCTION

Steels of a system $Fe-(\sim 29Mn)-(\sim 9Al)-(\sim 1C)-(\sim 1Si)$ are favourable to the magnetic investigation. The reason is that after quenching they have a structure of non-magnetic solid solution with FCC lattice (the magnetic permeability is $\mu \leq 1.0$ gauss/oersted). However, the aging process in the temperature range 290–800 °C leads to the decomposition of this solid solution. As this takes place, particles of ordered K-phase arise[1–7] which is carbid $(Fe, Mn)_3AlC_x$ and some magnetic properties appear. For example, an extensively used aging regime, at 550 °C during 16 hours, gives the samples with the magnetic permeability $\mu \approx 4$ gauss/oersted. However, up to our knowledge, there is no information till the moment about the investigation of magnetic properties of steels structure under different aging regimes (with changing of the temperature and of the duration of the isotermic exposure).

The early stage of the process of the aging of steels is a spinodal decomposition which occurs over all grain volume simultaneously. The free energy falls smoothly therewith and the composition of precipitations changes continuously. Orientation of the transformation products is determined by the initial lattice orientation, by the elastic constants matrix, by the coherent stress values and by the volume part of the precipitations[8–15]. The particles of magnetic phase have a spherical form at early stages of the aging process. The diffusing redistribution of impurity elements takes place between the initial solid solution lattice and precipitated particles which leads to the increasing of the mismatch parameter of their lattices and to the rise of elastic stress. As a result the magnetic particles take the form of parallelepiped. Also the regularity of the space distribution of these particles is built up: they are aligned along the elastic-soft cristallographic axis $<100>_\gamma$. The chains of particles and afterwords some flat blocks arise along the planes $\{100\}_\gamma$ which sizes increase with the increasing of temperature and of aging period. These flat blocks are similar to some right-angle nets where the particles are embedded at specific sites in the right-angle tetragonal lattice[16–18]. It has to be noted that the distances between the particles do not depend on their sizes. These distances are 5 nm in one direction and 3.5 nm in the other direction. The

blocks under consideration are arranged at some distance (50 nm) from each other along the lines $<100>_\gamma$ and also form a periodic structure. The general space distributions of magnetic particles have, on the average, cubic symmetry and consist of fragments with different orientation of the tetragonal axis "C"[16–18].

With the advent of the new high-resolution imaging technique magnetic force microscopy (MFM) should be mentioned primarily as a promoting tool for the analysis of magnetic microstructures (see, e.g., the monograph 19 and references therein). In particular, this (MFM) method was recently used for investigation of the micromagnetism of submicrometer magnetic particles[20,21].

This paper presents the experimental and theoretical results for atomic force microscopy (AFM) investigation of steels magnetic structure. The measurements were performed by the atomic force microscope of Ref. 22 used in the MFM regime. The paper is organized as follows. The general model for calculation of the magnetic force between the tip and the magnetic regions of a sample is presented in Sec. 2. Sec. 3 contains the examination of the van der Waals forces in determining the topography of the sample at small distances of order of 10 nm. The investigation of the MFM lateral resolution for the magnetic structures under study is the subject of Sec.4. Sec. 5 contains the description of experimental results obtained for two different aging regimes (550 °C – 16 hours and 700 °C – 5 hours) for the steel $Fe-28Mn-8.5Al-1C-1.4Si$. This section contains also the calculational results of magnetic and van der Waals forces which are compared with the experiment. In Sec. 6 we discuss the application of MFM method to the investigation of magnetic structure of steels under consideration.

II. MAGNETIC FORCE BETWEEN A TIP AND MAGNETIC REGIONS OF A SAMPLE

There are different approaches to calculation of magnetic force between the MFM tip and the magnetic sample. In particular, the force acting on the MFM tip (see, e.g., Refs.

23–25) or on the sample[26,27] can be calculated. We follow here the approach of Ref. 23 and calculate the force acting on the MFM tip by the magnetized steel sample. It is assumed that the magnetization of the tip does not influence on the sample magnetization and vice versa.

Experimental results discussed below were obtained by vertical magnetization of the sample along z-axis, parallel to the tip axis. The vertical component of the force acting on the MFM tip is expressed by[26–28]

$$F_z = -\int\limits_{V_t} M^{(t)}(\boldsymbol{r}) \frac{\partial H_z^{(s)}(\boldsymbol{r})}{\partial z}\, d^3r, \tag{1}$$

where $M^{(t)}$ is the magnetization of a tip volume element (the tip is magnetized along z-axis), $H_z^{(s)}$ is the z-component of the sample magnetic stray field at the position of the corresponding tip volume element. The integration on the right-hand side of Eq. (1) is done over the whole volume of the tip. Let us consider the magnetization of the sample unit volume $M^{(s)}$. It is reasonable to assume that the magnetization $M^{(s)}$ depends only on the position of this unit volume at the surface and does not depend on the depth. Then the general expression for the magnetic field produced by the sample has the form (the z-coordinate of the sample surface is chosen to be equal to zero)

$$H_z(\boldsymbol{r}) = \int\limits_{S^{(s)}} dx'dy' M^{(s)}(x',y') \left\{ \frac{z}{\left[(x-x')^2+(y-y')^2+z^2\right]^{\frac{3}{2}}} - \frac{z+D_s}{\left[(x-x')^2+(y-y')^2+(z+D_s)^2\right]^{\frac{3}{2}}} \right\}, \tag{2}$$

where D_s is the thickness of magnetic layer on the surface. The integration on the right-hand side of Eq. (2) is over the surface of the sample.

We may simulate the magnetic structure of the steels under investigation as the right-angle periodic lattice of the magnetic rectangular parallelepipeds with the sizes $D_x^{(m)} \times D_y^{(m)} \times D_s$. The periods of this surface lattice are D_x, D_y. The quantity $M^{(s)}$ as a function of the surface point coordinates is given here by an expansion in the Fourier series (the origin is located on the sample surface at the center of magnetic region)

$$M^{(s)}(x',y') = \sum_{k,n=0}^{\infty} M_{kn}^{(s)} \cos\left(2\pi k\frac{x'}{D_x}\right)\cos\left(2\pi n\frac{y'}{D_y}\right), \tag{3}$$

where

$$M_{00}^{(s)} = m_s\frac{D_x^{(m)}}{D_x}\cdot\frac{D_y^{(m)}}{D_y}, \qquad M_{k0}^{(s)} = m_s\frac{2}{\pi k}\frac{D_y^{(m)}}{D_y}\sin\left(\pi k\frac{D_x^{(m)}}{D_x}\right),$$
$$M_{0n}^{(s)} = m_s\frac{2}{\pi n}\frac{D_x^{(m)}}{D_x}\sin\left(\pi n\frac{D_y^{(m)}}{D_y}\right), \qquad k,n = 1,2,\ldots,$$
$$M_{kn}^{(s)} = m_s\frac{4}{\pi^2 kn}\sin\left(\pi k\frac{D_x^{(m)}}{D_x}\right)\sin\left(\pi n\frac{D_y^{(m)}}{D_y}\right),$$

and m_s is the unit volume magnetization of the magnetic phase generated during the steel aging process.

Using the expansion (3) we calculate the integrals on the right-hand side of Eq. (2). It should be noted that the sizes of magnetic phase particles and even of blocks of these particles are considerably less than the size of the steel sample surface. On this basis, we can integrate over the infinite plane instead of integrating over the sample surface. (Strictly speaking, results below are valid for the regions near the center of the sample.) Then, following Ref. 29, we obtain the result for magnetic field

$$H_z^{(s)}(x,y,z) = H_z^{(0)} + 2\pi\sum_{k,n=0}^{\infty}(1-\delta_{k0}\delta_{n0})M_{kn}^{(s)} \tag{4}$$
$$\times\, \mathrm{e}^{-\gamma_{kn}z}\left(1-\mathrm{e}^{-\gamma_{kn}D_s}\right)\cos\left(\gamma_{k0}x\right)\cos\left(\gamma_{0n}y\right),$$

where

$$\gamma_{kn} = 2\pi\sqrt{\frac{k^2}{D_x^2}+\frac{n^2}{D_y^2}}.$$

The dependence on δ-symbols on the right-hand side of Eq. (4) removes the item of the magnetization $M_{00}^{(s)}$ which was taken into account in the averaged magnetic field $H_z^{(0)}$ of the sample. Samples under investigation are realized as the cylinders with the radius R_s and the height h_s. Then it is easy to see that the averaged magnetic field above the sample surface is

$$H_z^{(0)}(z) = 2\pi\beta_V m_s \left[\frac{z+h_s}{\sqrt{R_s^2+(z+h_s)^2}} - \frac{z}{\sqrt{R_s^2+z^2}} \right], \tag{5}$$

where β_V is the part of the sample volume occupied by the precipitated magnetic phase.

In order to calculate the force F_z defined by Eq. (1) a tip model has to be chosen. The currently used model in AFM is a paraboloidal tip (see, e.g., Refs. 30,31) defined by the apex curvature radius. However this choice leads to cumbersome calculations. A truncated pyramid is mathematically much more convenient and may be used as a good approximation of a paraboloidal tip in the MFM simulations[24,32]. The model used in this work is shown in Fig. 1 with the corresponding notations. Calculating the force F_z, we have to integrate over the volume of magnetic coating of the tip. Substituting the magnetic field as defined by Eq. (4) into the right-hand side of Eq. (1) and integrating[33], one gets the result

$$\begin{aligned} F_z(x_0,y_0,z_0) &= F_z^{(0)} + M^{(t)} \\ &\times \left[\sum_{k=1}^{\infty} M_{k0}^{(s)} \mathrm{e}^{-\gamma_{k0} z_0} \left(1-\mathrm{e}^{-\gamma_{k0} D_s}\right) Q_{k0}^{(1)} \cos\left(\gamma_{k0} x_0\right) \right. \\ &+ \sum_{n=1}^{\infty} M_{0n}^{(s)} \mathrm{e}^{-\gamma_{0n} z_0} \left(1-\mathrm{e}^{-\gamma_{0n} D_s}\right) Q_{0n}^{(1)} \cos\left(\gamma_{0n} y_0\right) \\ &\left. + \sum_{k,n=1}^{\infty} M_{kn}^{(s)} \mathrm{e}^{-\gamma_{kn} z_0} \left(1-\mathrm{e}^{-\gamma_{kn} D_s}\right) Q_{kn}^{(2)} \cos\left(\gamma_{k0} x_0\right) \cos\left(\gamma_{0n} y_0\right) \right], \end{aligned} \tag{6}$$

where the following notations are used

$$\begin{aligned} Q_{kn}^{(1)} &= \frac{8\pi}{\gamma_{kn}^2} \frac{1}{1+\beta^2} \left[P^{(1)}\left(\gamma_{kn} L_t\right) - \mathrm{e}^{-\gamma_{kn}\Delta} P^{(1)}\left(\gamma_{kn} L_t'\right) \right], \\ Q_{kn}^{(2)} &= \frac{2\pi\gamma_{kn}}{\gamma_{k0}\gamma_{0n}} \left[P_{kn}^{(2)}(L_t) - \mathrm{e}^{-\gamma_{kn}\Delta} P_{kn}^{(2)}(L_t') \right]. \\ P^{(1)}(x) &= \left(\beta x + \frac{2\beta^2}{1+\beta^2} \right) \cos x + \left(x + \beta \frac{1-\beta^2}{1+\beta^2} \right) \sin x, \\ P_{kn}^{(2)}(x) &= \sum_{p=1}^{2} (-1)^p \frac{\gamma_{kn} \cos(\alpha_{kn}^{(p)} x) - \alpha_{kn}^{(p)} \beta \sin(\alpha_{kn}^{(p)} x)}{\gamma_{kn}^2 + \beta^2 (\alpha_{kn}^{(p)})^2}, \\ \alpha_{kn}^{(1)} &= \gamma_{k0} + \gamma_{0n}, \qquad \alpha_{kn}^{(1)} = \gamma_{k0} - \gamma_{0n}, \qquad \beta = \tan\varphi. \end{aligned}$$

The coordinates x_0, y_0 in Eq. (6) define the tip apex center, and z_0 is the distance between the tip and the sample surface. It has to be noted that in the calculation of the force (6) the

small contribution of the upper end of the tip was neglected (for the calculational results see Sec. 5).

III. AFM TOPOGRAPHY

The AFM topography at the distances $\approx 10\,\mathrm{nm}$ is determined essentially by the van der Waals interaction. The exact calculation of the van der Waals forces is possible to be performed only for configurations with a high symmetry[34]. In all other cases approximative methods has to be used. The straightforward approximative method is the perturbation theory for the Green function in the medium with respect to a small parameter. Unfortunately, this method is quite complicated and can not be used for the surfaces which are not planes. So the ordinary method of the additive potentials is commonly used for the AFM simulations (see, e.g., Refs. 30,31,35,36). We assume that the potential energy of the tip-sample interaction is equal to the sum of the interatomic van der Waals potentials over all atoms of the sample and of the tip:

$$U(d) = -N_1 N_2 \int\limits_{V_s} d\boldsymbol{r}_1 \int\limits_{V_t} d\boldsymbol{r}_2 \frac{A}{|\boldsymbol{r}_1 - \boldsymbol{r}_2|^6}, \tag{7}$$

where the integrations are over the volumes of the sample (V_s) and of the tip (V_t), $N_1(N_2)$ is the number of the sample (tip) atoms per unit volume, A is the constant of non-retarded van der Waals interaction, and d is the distance between the AFM tip and the sample. The integrals on the right-hand side of Eq. (7) give the proper dependence of U on d. However due to the screening effects the value of the coefficient in this dependence comes out to be larger than the correct one[34].

To take into account the screening effects it is convevient to consider the so-called "renormalized"[30,31,35] potential $U_R(d) = U(d)/K$. The renormalization constant K is chosen as the ratio of the van der Waals force potentials between two infinite plane parallel plates obtained by the simple summation of the interatomic potentials and by the exact calculation $K = \pi^2 A N_1 N_2 / H$, where H is the Hamaker constant[34]. The renormalized potential energy

can now be expressed by

$$U_R(d) = -\frac{H}{\pi^2}\int\limits_{V_s} d\boldsymbol{r}_1 \int\limits_{V_t} d\boldsymbol{r}_2 \frac{1}{|\boldsymbol{r}_1 - \boldsymbol{r}_2|^6}. \tag{8}$$

The relative error of the potential $U_R(d)$ does not exceed 9% for the configuration of an arbitrary dielectric sample over a plane[37].

The vertical component of the force, acting on the AFM tip, is calculated as

$$F_z = -\frac{\partial U_R(d)}{\partial d}. \tag{9}$$

Eq. (9) gives the attractive force acting on the AFM tip. The contribution of the exchange repulsive forces can be neglected for the values $d > 4$ Å.

Note that F_z strongly depends on the model of AFM tip used for simulations[36]. Approximating the tip by a paraboloid, a cone or a truncated pyramid and calculating the force between each of them and the infinitely large plane plate, we obtain different dependences on the distance d, i.e. $F_z^p = -HC_p/d^2$, $F_z^c = -HC_c/d$ and $F_z^{tp} = -HC_{tp}/d^3$ respectively. The constants $C_{p(c,tp)}$ depend on the geometrical parameters of the corresponding tips.

A real steel sample has different roughness on its surface, and the Hamaker constant may be different for the different regions of sample. So simulation of the real topography images is a complicated problem due to the mathematical difficulties connected with the integration contained in Eq. (8) and also to the large uncertainty with which the Hamaker constant is known. It has to be noted that the absolute value of the distance between the AFM tip and the sample surface is not precisely known. The last two points are essential for a good simulation of topography surface. As a first approximation, roughness on the sample surface can be modeled by steps (see Fig. 2, where a model situation is shown). In this case integration on the right-hand side of Eq. (8) can be performed and the force F_z becomes[38]

$$\begin{aligned} F_z = -H^{(1)}\frac{R_t}{6}\Big[\frac{1}{d^2} - I(l,d) + I(l+L_1,d) - I(l+L_1+L_2,d) \\ + I(l+L_1+L_2+L_3,d)\Big] + H^{(2)}\frac{R_t}{6}\big[I(l,d+h) - I(l+L_1,d+h) \\ + I(l+L_1+L_2,d+h) - I(l+L_1+L_2+L_3,d+h)\big], \end{aligned} \tag{10}$$

where $H^{(1,2)}$ are the Hamaker constants for the different pairs of materials, and R_t is the curvature radius of the paraboloidal tip. The other distances are determined in accordance with Fig. 2, and also the notation is used

$$
\begin{aligned}
I(A,B) = {} & \frac{1}{4B^3}(A^2+2R_tB)^{-\frac{3}{2}}[4A^2+(R_t+2B)^2]^{-\frac{1}{2}} \\
& \times \Big\{ \mathrm{sign}A \left(7A^2R_tB + 4B^3R_t + 4B^2R_t^2 + 2A^4 - 2B^2A^2 - 8B^4\right) \\
& \times \left[2B^2 + BR_t + A^2 - |B|\sqrt{4A^2+(R_t+2B)^2}\right]^{\frac{1}{2}} \\
& + A\sqrt{A^2+2R_tB}\left(2B^2 - 5BR_t - 2A^2\right) \\
& \times \left[2B^2 + BR_t + A^2 + |B|\sqrt{4A^2+(R_t+2B)^2}\right]^{\frac{1}{2}} \Big\}. \qquad (11)
\end{aligned}
$$

There is a special interest during last years to the investigation of the van der Waals forces (see, e.g., Refs. 36,39 and references therein). Unfortunately the lack of knowledge of the exact values of the Hamaker constants makes it impossible to give a good quantitative simulation of the AFM topography. At the same time a qualitative agreement is obtained between the theory and experiment (see Sec. 5).

IV. INVESTIGATION OF LATERAL RESOLUTION

Studies of the structures of magnetic domain walls have shown (see, e.g., Refs. 25,32) that the MFM lateral resolution is roughly equal to the distance between the tip and the sample surface z_0 when this distance is greater than the width of the tip apex ($z_0 > 2L_t$)[32]. For $z_0 < 2L_t$ a more detailed analysis of geometrical and magnetic structure of the tip is necessary.

During the aging process of steels under consideration two types of magnetic structure are obtained. The first structure is formed by the magnetic particles having the magnitization $M^{(s)}$ per unit volume. The second type is formed by the blocks of these magnetic particles which arise during the aging process. We assume a block as a "magnetic" region with the magnetization $\bar{M}^{(s)}$ per unit volume, and $\bar{M}^{(s)} = p_V M^{(s)}$, where p_V is the part of the block volume occupied by the magnetic phase.

If the distance between the AFM tip and the sample surface is much smaller than the size of a block, the first type of the structure can be considered as the main one. Then, we have to use on the right-hand sides of Eqs. (4) and (6) the quantities $D_x = D_x^{(m)} + d_x$, $D_y = D_y^{(m)} + d_y$, where $D_x^{(m)}$, $D_y^{(m)}$ are the sizes of magnetic particle, $d_x = 5\,\mathrm{nm}$, $d_y = 3.5\,\mathrm{nm}$ are the distances between them. In this case, it can be assumed that the size of a block is infinitely large, i.e. that the sample has the block magnetic structure over all its volume.

If the distance between the AFM tip and the sample surface is of the order of block's size, the second type of the structure can be considered as the main one, and in this case we take the block as being some effective "magnetic phase". As a first approximation, the different orientations of the blocks are not taken into account . Then the quantities $D_x^{(m)}$, $D_y^{(m)}$ on the right-hand sides of Eqs. (4) and (6) are equal to the size of the block. The distance between the blocks $d_x \approx d_y \approx 50\,\mathrm{nm}$ must be taken into account by calculation of D_x, D_y.

An inspection of the right-hand side of Eq. (4) shows that it is difficult to imagine the possibility of magnetic structure observation at $z_0 > D_x, D_y$. In fact, in this case, even the contribution of the first harmonics is small due to the exponential dependence on z. So, the field component $H_z^{(s)}$ is nearly independent on z and the force F_z is equal to zero. Note that it is convenient to investigate the lateral resolution step by step. The first step is using Eq. (4) to check if the magnetic structure of the sample is well represented by the magnetic field structure at a distance z. The second step must be performed using Eq. (6). It consists in checking how the force acting on the MFM tip represents the structure of the magnetic field.

The numerical simulations were performed using Eq. (4) for different sizes of magnetic particles. They were assumed to have a cubic form with the size $D_x^{(m)} = 5$, 10, 15 nm. The distances between these particles are those corresponding to the first type of the sample magnetic structure. It is shown that the corresponding magnetic field is nearly independent on x and y at $z > 10\,\mathrm{nm}$. We can see that the relative amplitude of the magnetic field oscillations decreases with increasing of d. The reason is that the narrow non-magnetic

regions between the magnetic particles can not influence essentially on the resulting magnetic field when the size of these particles increases in such a way that $D_x \approx D_x^{(m)}$. The obtained results are in a good agreement with the estimations of the lateral resolution given in Ref. 25.

V. RESULTS AND DISCUSSIONS

The experimental study was made by using a TopoMetrix Scanning Probe Microscope TMX2010 Discoverer with a force sensor operating in non-contact mode. The scanner used in this experiment was a piezoelectric tripoid of $70\,\mu$m with a commercial cantilever of $k = 2.0\,$N/m and a paramagnetic tip having a magnetic Co coating with thickness $\Delta \approx 10\,$nm. The curvature radius of the paraboloidal tip is estimated as $\approx 10\,$nm. The magnetization of the tip is along its vertical axis by the field 1 kgauss.

The steel chosen for the investigations has a typical composition $Fe - 28Mn - 8.5Al - 1C - 1.4Si$. Samples obtained after two different aging regimes 550 °C – 16 hours and 700 °C – 5 hours are considered. The reason of this choice is that these regimes give structures characterized by a different extent of dispersion and by a different space distribution of precipitated K-phase. The samples under investigation have a cylindrical form with a radius $R_s \approx 0.5\,$cm and a height $h_s \approx 4\,$mm. The surface has been chemically etched, for 40 sec, in an ultrasonic bath with Nital 2% (2% of nitric acid and 98% of ethyl alcohol). The acid acts only on the matrix solution around the magnetic particles producing an enhancement on their images. In order to locate the regions with the $\{100\}_\gamma$ orientation a Baush and Lomb model 2600-00 optical microscope was coupled to the AFM stage. It should be noted that the magnetic characteristics are unknown for both decomposition products and matrix solid solution. This situation adds complexity to the choice of magnetization parameters of the sample and of the scanning tip and consequentlly to the elaboration of optimal MFM operating conditions. Prior to any MFM imaging the samples were magnetized at magnetic field of 10 kgauss in the direction perpendicular to the surface.

Fig. 3,a shows the topography of the sample under the aging regime of 700 °C during

5 hours. The image was obtained in constant gradient force AFM operating mode. Fig. 3,b shows the line of constant force (solid curve) when the direction of the scanning is along the line indicated in Fig. 3,a. The dotted curves seen in Fig. 3,b are the theoretical constant force lines. They were obtained by the solution of non-linear equation $F_z = F_c$. The curve 1 corresponds to the situation when the van der Waals force is solely responsible for the form of the line. The force F_z is calculated according to Eq. (10) with the values of parameters $R_t = 20\,\text{nm}$, $L_1 = L_3 = 50\,\text{nm}$, $L_2 = 70\,\text{nm}$, $h = 30\,\text{nm}$ (see Fig. 2). We assume also that $H^{(1)} = H^{(2)}$. The value of F_c is chosen to be equal to the value of the van der Waals force at the distance of 15 nm above the infinite plane. In this case the contour of the constant force line is determined by the surface relief only. The curve 2 corresponds to the situation when not only the van der Waals force but also the magnetic one act on the AFM tip. Then F_z can be calculated as the sum of the forces given by Eqs. (10) and (6). In order to obtain the curve 2, we calculate the van der Waals force with the same values of R_t and $L_{1(2,3)}$ as before but for a lesser depth of the surface relief ($h = 10\,\text{nm}$). Since there is no exact information on the geometrical parameters of the tip, the magnetization of the tip and of the sample and the values of Hamaker constants, it was assumed that the force amplitudes of the first harmonics in Eq. (6) are equal to $F_c/2$. The curves of Fig. 3,b show that our model can be used for the interpretation of the sample surface topography.

Fig. 4,a shows the MFM image of the corresponding magnetic structure. It was obtained in a constant height $z_0 = 112 \pm 10\,\text{nm}$ from the constant gradient mapping of the surface. This image is the result of the magnetic interaction. Note that there is a correlation between the images of Fig. 3,a and Fig. 4,a. In the Fig. 4,b the force contour is shown by the solid curve when the scanning direction is along the line indicated in Fig. 4,a (1 nA along the vertical axis corresponds to the force of 1.11 nN). The results of the simulation according to Eq. (6) are shown by the dotted curve. It must be noted that, since the magnetization of the sample and the actual parameters of the tip are known with low accuracy, this simulation is of qualitative character. We have calculated the relative force $F_z/F_z^{(0)}$ which does not depend on the magnetization parameters $M^{(t)}$ and m_s. For this calculation it is assumed

that $D_x^{(m)} = 70\,\mathrm{nm}$, $D_y^{(m)} = 300\,\mathrm{nm}$, $D_s = 50\,\mathrm{nm}$, $z_0 = 100\,\mathrm{nm}$, $L_t' = 10\,\mathrm{nm}$, $\varphi = 30°$, and $\beta_V = 0.25$. Then the normalization of the calculated force is used in such a way that $F_z^{(0)}$ is equal to the mean value of the measured force. After this normalization the theoretical and experimental results are in a good agreement.

Let us now turn out to the results obtained for the sample under the aging regime 550 °C during 16 hours. Fig. 5 shows the image obtained by MFM. In this case the magnetic structure is much smaller. We can not exactly determine the magnetic contribution since, close to the surface, it is of the same order of the van der Waals forces.

VI. CONCLUSION

In this work we report the investigation of the MFM response to magnetic structure in steels of a system $Fe - Mn - Al - C$ which appears to be caused by decomposition of the solid solution during aging process. A theoretical model has been developed for the MFM image. This model gives the possibility to describe the structures formed by the particles of magnetic phase and by the blocks of such particles which arise during the aging process. The investigation of the MFM lateral resolution also was performed in the context of this model. It was shown that the MFM response represents the blocks of magnetic phase particles at the typical distancies of ($z_0 \sim 100\,\mathrm{nm}$) between the AFM tip and the sample. The model developed in this paper is suitable for the description of the measured MFM response and the results of corresponding calculations are in good agreement with experiment. However, in order to obtain a detailed quantitative simulation of magnetic structure better knowledge of the geometrical and magnetic parameters of the MFM tip is needed.

The calculation of the van der Waals forces was also discussed because they are essential for the understanding of the AFM topography. We have considered a model which gives the possibility of some qualitative interpretation in terms of the imaged sample surface topography. Conditions for a good MFM imaging of such steels were also formulated which should be fulfilled to image its details.

ACKNOWLEDGMENTS

This work is partially supported by Conselho Nacional de Desenvolvimento Científico e Technológico (CNPq).

List of Captions

Fig. 1. The model of the MFM tip.

Fig. 2. The model of the sample for the calculation of the van der Waals force.

Fig. 3. Topography (a) and the constant force line (b, the solid curve) for the sample under the aging regime of 700°C during 5 hours. The dotted curves (b) represent the theoretical results for the different models of the sample. Both images have a scan area of $1\mu m^2$

Fig. 4. MFM image (a) and the line of magnetic force (b, the solid curve) for the sample under the aging regime of 700°C during 5 hours. The dotted curve (b) represents the theoretical results. The scan area for both images are $1\mu m^2$.

Fig. 5. Topography (left) and MFM images for the sample under the aging regime of 550°C during 16 hours. Both images have a scan area of $1\mu m^2$.

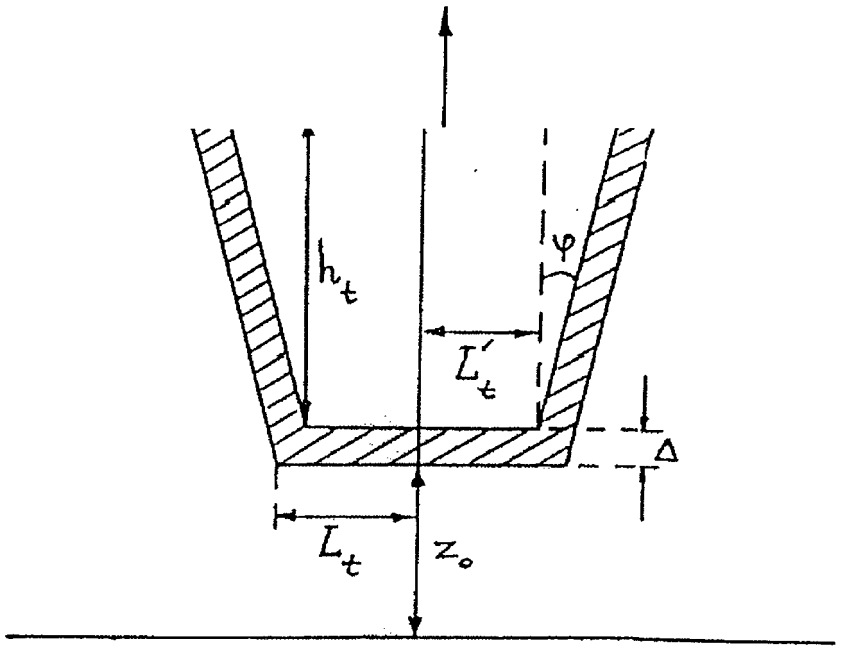

Figure 1

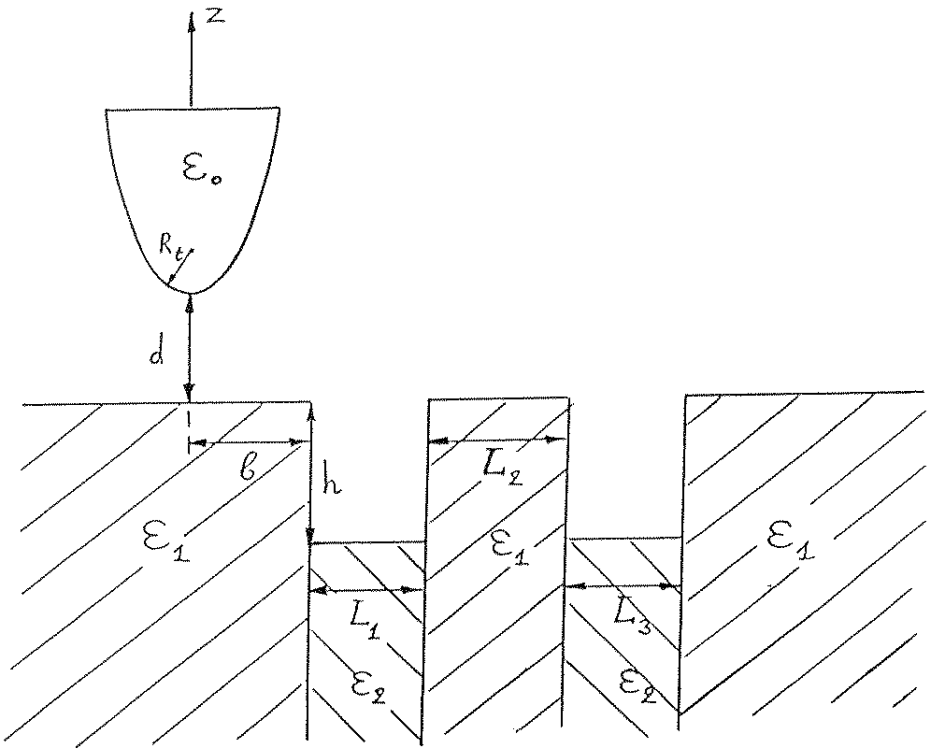
z
ε_0
R_t
d
b
h
ε_1
L_1
ε_2
L_2
ε_1
L_3
ε_2
ε_1

Figure 2

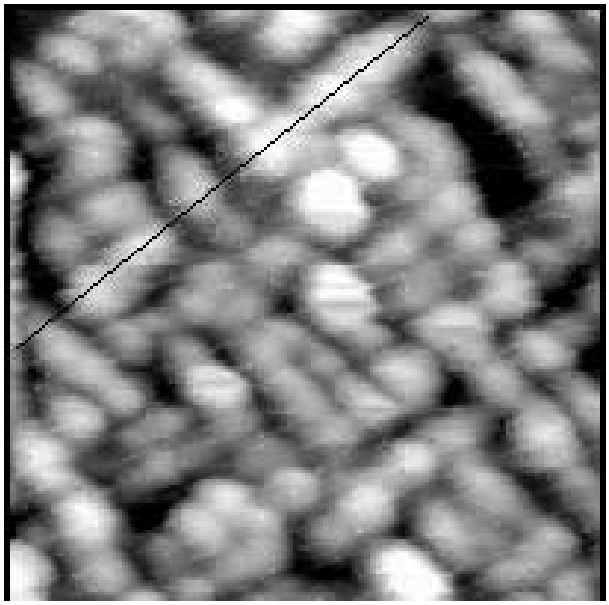

Figure 3a

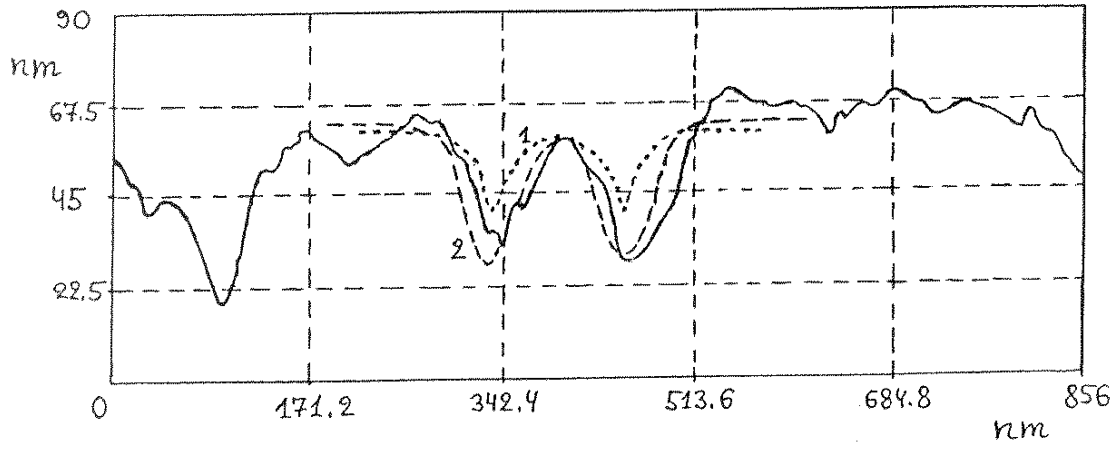

Figure 3b

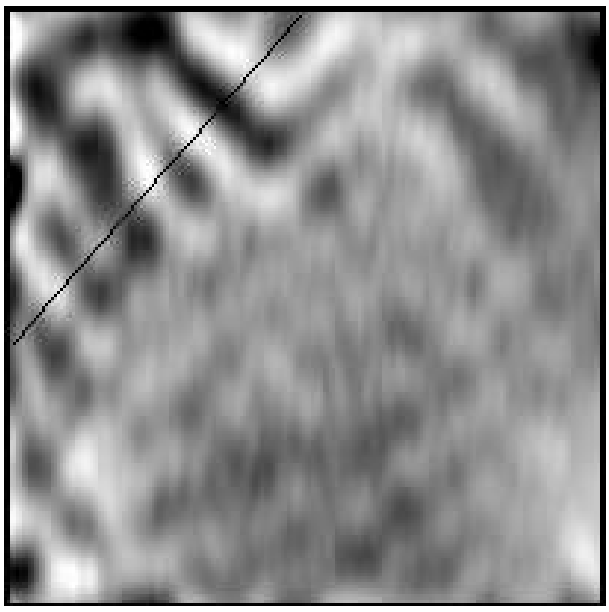

Figure 4a

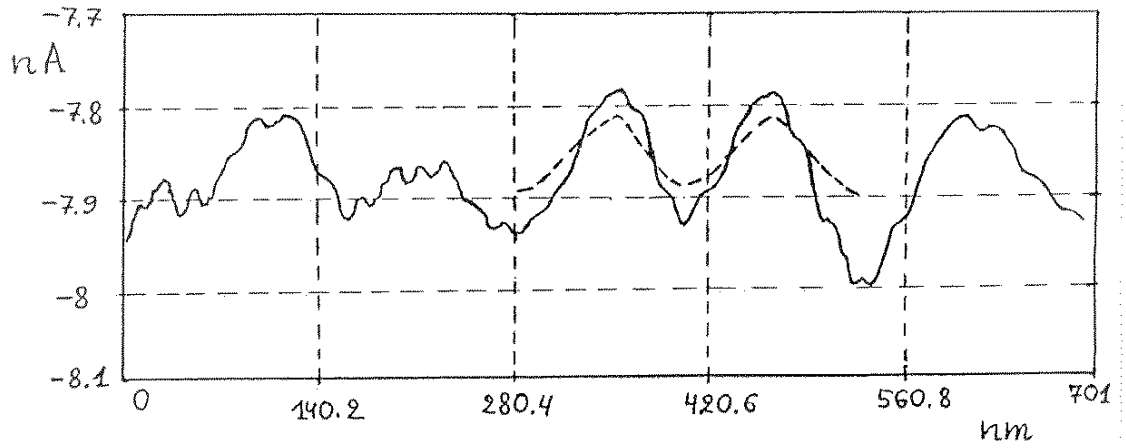

Figure 4b

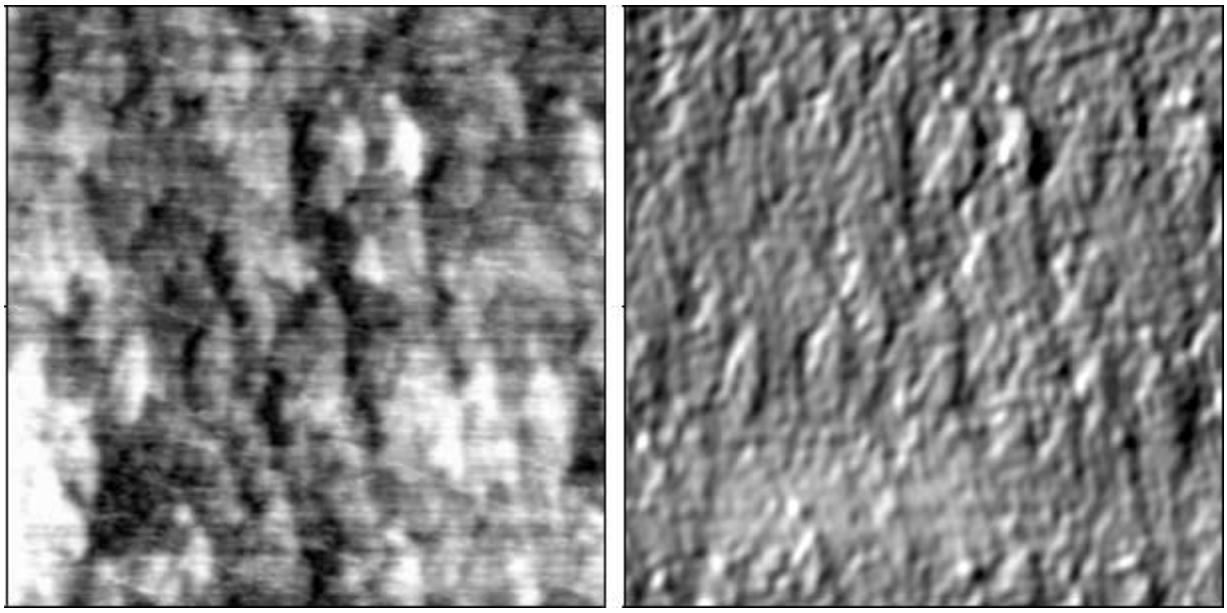

Figure 5

REFERENCES

* on leave from North-West Polytechnical Institute, St.Petersburg, Russia

** present address: Departamento de Física, Universidade Federal da Paraíba, Caixa Postal 5008, CEP 58.059-970 João Pessoa, Pb, Brazil

*** on leave from Institute of Aviation Materials (VIAM), Moscow, Russia

[1] J.K. Ham and R.E. Cairns, Prod. Eng. **29**, 50 (1958).

[2] G.L. Kayak, Met. Sci. Heat Treatment **2**, 95 (1969).

[3] M.F. Alekseyenko, G.S. Krivonogov, L.G. Kozyreva, A.M. Kachanova, and L.V. Arapova, Metal. Sci. Heat Treat. N 3, 187 (1972).

[4] G.S. Krivonogov, M.F. Alekseyenko, and G.G. Solov'yeva, Phys. Met. Metallogr. **39**, 86 (1975).

[5] N.A. Storchak and A.G. Drachinskaya, Phys. Met. Metallogr. **44**, 123 (1977).

[6] W.B. Pearson, *Handbook of Lattice Spacing and Structures of Metals and Alloys*, v.1 (Pergamon Press, L., 1958).

[7] A.S. Palatnik, I.A. Tananko, and Yu.G Bobro, Kristallografiya **9**, 209 (1964).

[8] K.V. Chuistov, *Aging of Metallic Alloys* (Naukova Dumka, Kiev, 1974, in Rus.).

[9] A. G. Khachaturyan, *Theory of Structure Transformations in Solid Solutions* (Wiley, N.Y., 1983).

[10] A. Kelli and R. Nicolson, *Dispersion Harding* (Metallurgiya, Moscow, 1966, in Rus.).

[11] Yu.D. Tiapkin, in *Structural Mechanism of Phase Transformations of Metals and Alloys* (Nauka, Moscow, 1976, in Rus.), p.104.

[12] Yu.A. Bagaryatskii and Yu.D. Tyapkin, Kristallografiya **5**, 882 (1960).

[13] D.E. Laughlin and J.W. Cahn, Acta Met. **23**, 329 (1975).

[14] Ya.S. Umanskiy and Yu.A. Skakov, *Physics of Metals* (Atomizdat, Moscow, 1978, in Rus.).

[15] Yu.D. Tyapkin, Ann. Rev. Mater. Sci. **7**, 209 (1977).

[16] I.S. Kalashnikov, V.S. Litvinov, M.S. Khadyyev, and L.D. Chumakova, Phys. Met. Metallogr. **57**, 160 (1984).

[18] S.D. Karakishev, L.D. Chumakova, A.A. Senchenko, and I.S. Kalashnikov, Met. Sci. Heat Treat. N 8, 58 (1986).

[18] Yu.D. Tyapkin, E.U. Maliyenko, I.V. Gongadze, I.S. Kalashnikov, and S.M. Komarov, Phys. Met. Metallogr. **68**, 121 (1989).

[19] R. Wiesendanger, *Scanning Probe Microscopy and Spectroscopy* (Cambridge University Press, Cambridge, 1994).

[20] G.A. Gibson and S. Schultz, J. Appl. Phys. **73**, 4516 (1993).

[21] R.M.H. New, R.F.W. Pease, R.L. White, R.M. Osgood, and K. Babcock, J. Appl. Phys. **79**, 5851 (1996).

[22] R. Prioli, S.I. Zanette, and A.O. Caride, D.F.Franceschini and F.L.Freire, Jr., J. Vac. Sci. Technol. A **14**, 1 (1996).

[23] U. Hartman, J. Appl. Phys. **64**, 1561 (1988).

[24] A. Wadas and P. Grüter, Phys. Rev. B **39**, 12013 (1989).

[25] A. Wadas and H.-J. Güntherodt, J Appl. Phys. **68**, 4767 (1990).

[26] C.D. Wright and E.W. Hill, Appl. Phys. Lett. **67**, 433 (1995).

[27] C.D. Wright and E.W. Hill, Appl. Phys. Lett. **68**, 1726 (1996).

[28] T. Goddenhenrich, H. Lemke, M. Muck, U. Hartman, and C. Heiden, Appl. Phys. Lett. **57**, 2612 (1990).

[29] M. Bordag, G.L. Klimchitskaya, and V.M. Mostepanenko, Int. J. Mod. Phys. A **10**, 2661 (1995).

[30] Yu.N. Moiseev, V.M. Mostepanenko, V.I. Panov, and I.Yu. Sokolov, Phys. Lett. A **132**, 354 (1988); Sov. Phys. Tech. Phys. (USA) **35**, 84 (1990).

[31] M. Bordag, G.L. Klimchitskaya, and V.M. Mostepanenko, Surf. Sci. **328**, 129 (1995).

[32] R.B. Proksch, S. Foss, and E. Dan Dahlberg, IEE Trans. Magn. **30**, 4467 (1994).

[33] I.S. Gradshteyn and I.M. Ryzhik, *Table of Integrals, Series and Products* (Academic, New York, 1980).

[34] E.M. Lifshitz and L.P. Pitaevsky, *Statistical Physics, Part 2* (Pergamon, Oxford, 1980).

[35] V.M. Mostepanenko, V.I. Panov, and I.Yu. Sokolov, Tech. Phys. Lett. (USA) **19**, 251 (1993).

[36] C. Agento and R.H. French, J. Appl. Phys. **80**, 6081 (1996).

[37] M. Bordag, V.M. Mostepanenko, and I.Yu. Sokolov, Phys. Lett. A **187**, 35 (1994).

[38] E.V. Blagov, Yu.N. Moiseev, V.M. Mostepanenko, A.Yu. Musatenko, V.I. Panov, S.V. Savinov, and I.Yu. Sokolov, Rus. Phys. Tech. Phys. (USA) **39**, N1 (1994).

[39] E. Hult and A. Kiejna, Surf. Sci. **383**, 88 (1997).